Design of electromagnetic energy harvesters for large-scale structural vibration applications

Ian L. Cassidy*[a], Jeffrey T. Scruggs[a], and Sam Behrens[b]

[a]Dept. of Civil & Environmental Engineering, Duke University, Durham, NC, USA
[b]CSIRO Energy Centre, PO Box 330, Newcastle, New South Wales 2300, Australia

ABSTRACT

This paper reports on the design and experimental validation of transducers for energy harvesting from large-scale civil structures, for which the power levels can be above 100W, and disturbance frequencies below 1Hz. The transducer consists of a back-driven ballscrew, coupled to a permanent-magnet synchronous machine, and power harvesting is regulated via control of a four-quadrant power electronic drive. Design tradeoffs between the various subsystems (including the controller, electronics, machine, mechanical conversion, and structural system) are illustrated, and an approach to device optimization is presented. Additionally, it is shown that nonlinear dissipative behavior of the electromechanical system must be properly characterized in order to assess the viability of the technology, and also to correctly design the matched impedance to maximize harvested power. An analytical expression for the average power generated across a resistive load is presented, which takes the nonlinear dissipative behavior of the device into account. From this expression the optimal resistance is determined to maximize power for an example in which the transducer is coupled to base excited tuned mass damper (TMD). Finally, the results from the analytical model are compared to an experimental system that uses hybrid testing to simulated the dynamics of the TMD.

Keywords: Energy harvesting, vibration, mechatronics, impedance matching

1. INTRODUCTION

Large-scale electromechanical transduction in vibrating civil structures has a number of useful applications. Most immediate among these is their use in large scale energy harvesting applications, in which the vibratory energy in a structure, when excited by its surrounding environment, is converted and stored for use by electronic subsystems. Such environmental disturbances may include, for example, wind excitations on buildings, wave excitations on offshore structures, traffic-induced vibrations in bridges, and seismic events.[1–3] Such systems also have application in vehicles, including automotive suspensions[4] and railway systems.[5] The energy harvested from these vibrations can be used to power wireless sensing networks and other intelligent systems for structural health monitoring.[6–8] It can also be used to provide parasitic power for semiactive structural control devices, such as magnetorheological dampers.[9]

The last decade has seen a surge of interest in vibratory energy harvesting,[10,11] but most of this research has been motivated by vibration applications in the aerospace sector, and is focused on vibratory regimes characterized by frequencies above 10Hz, displacement oscillations on the order of millimeters, and power on the scale of milliwatts (or below). For such applications, piezoelectric transducers have been the dominant technology, although electrostatic[12] and electromagnetic[13] MEMS transducers have also seen significant attention. In contrast to these applications, the vibratory regime typical of a civil-scale structure oscillating in its fundamental mode is typically below 1Hz, and the available power can be on the kilowatt scale. Transducers to extract this energy must therefore be capable of extracting significant power from low-frequency, low-velocity oscillations. Operation in this vibratory regime thus requires very different electromechanical hardware than in higher-frequency, lower-power applications.

This paper reports on experiments conducted at Duke University in collaboration with the CSIRO Energy Centre, on the design and experimental characterization of an electromechanical transducer capable of generating

*Further author information: E-mail: ian.cassidy@duke.edu, Telephone: (919) 660-5200

Active and Passive Smart Structures and Integrated Systems 2011, edited by Mehrdad N. Ghasemi-Nejhad,
Proc. of SPIE Vol. 7977, 79770P · © 2011 SPIE · CCC code: 0277-786X/11/$18 · doi: 10.1117/12.880639

over 100W of power from sub-Hertz structural vibration, and with a force rating of 1kN. While this system is likely still a scaled-down version of a system which would be appropriate for full-scale civil structure applications, it does serve as a bench-scale demonstration of the technology. The basic conversion system consists of a back-driven precision ballscrew, which is coupled to the shaft of a three-phase, permanent-magnet synchronous machine. The machine terminals are interfaced with a three-phase active power electronic drive, which delivers harvested energy to a power bus. This work is an extension of the work in.[14]

In addition to the experimental validation of the concept, the paper makes a number of broader contributions. The first of these is an approach to the system-level design of this type of transducer, which accounts for the interdependency of the electronics, electronic controller, machine parameters, mechanical conversion system, and the characteristics of the structure into which the system is to be embedded. Another contribution is the derivation of an analytical expression for the average power generated, which can be used to determine the impedance matched resistive load for the case in which the transducer is attached to tuned mass damper (TMD). Several studies[15,16] have utilized power electronic drives to simulate impedance matched loads for piezoelectric energy harvesting applications. Our approach to designing the matched impedance takes the Coulomb friction present in the transducer into account. The analytical expression for average power generated is compared to our experimental system in which a TMD is simulated using hybrid testing.

2. DEVICE MODELING

An illustration of the electromechanical device to be characterized in this paper is illustrated in Fig. 1(a). Linear-to-rotational conversion is accomplished via a precision ballscrew. Such devices (as well as planetary roller screws) constitute one of the most efficient methods of linear-to-rotational conversion when power flow is in the direction from linear to rotational motion, and when high mechanical advantage is important. The particular ball screw mechanism used here is a Thomson EC3 unit. It has a lead of 16mm/rev, and a diameter of 16mm, resulting in a helical angle of approximately 17 degrees. The force rating on the screw is 7.2kN, well in excess of the force range for the experiment. The ballscrew is interfaced with the motor shaft via a timing belt with a 1:1 ratio. The configuration shown, in which the motor is placed in tandem with the screw, was chosen because it allowed for easier mounting of the device at either end via clevis brackets. However, a custom configuration in which the motor shaft is mounted directly to the rotating screw, and which also permits a clevis bracket to be mounted behind the motor housing, would reduce the need for the timing belt and also reduce Coulomb friction in the system by reducing side-loads on both rotating shafts.

The linear velocity $\dot{x}$ of the device is related to its mechanical angular velocity $\dot{\theta}_m$ via the lead conversion; i.e.,

$$\dot{x}(t) = l\dot{\theta}_m(t) \tag{1}$$

where l is in m/rad. The linear-to-rotational conversion of the ballscrew can be modeled as relating the linear

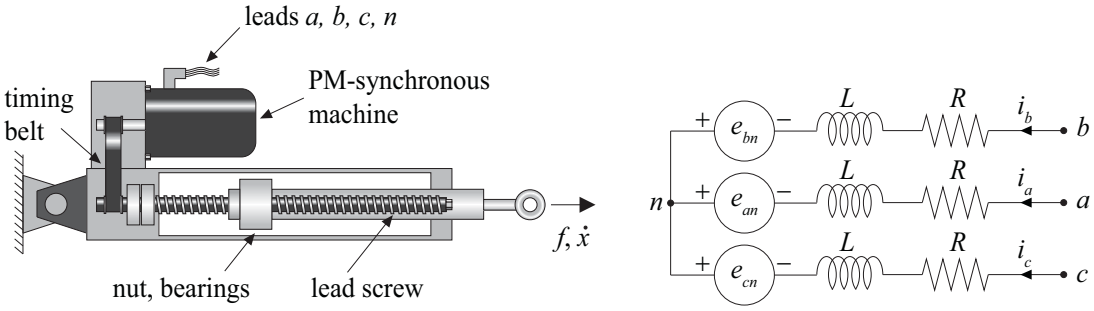

(a) Ballscrew transducer illustration (b) Electrical schematic

Figure 1. Electromechanical transducer, consisting of a back-driven ballscrew and a permanent magnet synchronous machine.

force f to the electromechanical f_e of the motor, via the equation

$$f(t) = h\left(f\dot{x}\right)\left(f_e(t) + \frac{J}{l^2}\ddot{x}(t) + \frac{B}{l^2}\dot{x}(t)\right) + f_d\left(x(t), \dot{x}(t)\right) \tag{2}$$

where the sign convention is that f and v have the same directional sense. In the above expression, B and J are the rotational viscosity and inertia, respectively, of the combined motor shaft and screw, f_d is a damping force associated with the friction losses in the device, and h is

$$h\left(f\dot{x}\right) = \begin{cases} \frac{1}{\eta} & : \quad f\dot{x} \geq 0 \\ \eta & : \quad f\dot{x} \leq 0 \end{cases} \tag{3}$$

where $\eta \in (0, 1)$ is the efficiency of the screw conversion itself. To very good approximation, η can be considered as an increasing function of the helical angle of the screw, and is generally above 0.9 for quality ballscrews with helical angles above about 6 degrees. It should be noted that backlash in the system is insignificant.

The motor itself is a Kollmorgen AKM42E permanent-magnet synchronous motor. The motor is three-phase and has a polarity $p = 5$. The choice of a rotary three-phase AC motor (as opposed to a rotary DC motor or a linear motor) was made based on practical considerations. Generally, for motors with comparable power ratings, ones with higher velocity (and lower torque) capability tend to be less massive, as they require less iron to sustain the necessary magnetic field. This becomes even more pronounced in the comparison between rotary and linear motors of comparable power ratings. Additionally, rotary synchronous three-phase machines are almost always more efficient as power generators, because they can generate a larger back-EMF for a given mechanical velocity, while also possessing a lower coil resistance.

The internal voltages (i.e., back-EMFs) for phases a, b, and c, relative to the neutral node n, are a function of the electrical angle $\theta_e = p\theta_m$, as

$$e_{an}(t) = K_e\dot{\theta}_e(t)\cos\left(\theta_e(t)\right) \tag{4a}$$

$$e_{bn}(t) = K_e\dot{\theta}_e(t)\cos\left(\theta_e(t) + \frac{2\pi}{3}\right) \tag{4b}$$

$$e_{cn}(t) = K_e\dot{\theta}_e(t)\cos\left(\theta_e(t) - \frac{2\pi}{3}\right) \tag{4c}$$

where K_e is the back-EMF constant. Let the line-to-neutral voltages at the terminals of the three phases be v_{an}, v_{bn}, and v_{cn}. Ultimately, these voltages will be imposed by the circuitry to be attached to the motor. Then the line current emanating from phase a, as seen in Fig. 1(b), of the machine evolves according to

$$\tfrac{d}{dt}i_a(t) = \frac{1}{L}\left(-Ri_a(t) + v_{an}(t) - e_{an}(t)\right) \tag{5}$$

where L and R are the line-to-neutral inductance and resistance, respectively, of the motor. Analogous equations hold for the other two phases.

Consider the case in which the transducer will ultimately be used in an application as shown in Fig. 2. As shown, the transducer is attached to a single-degree-of-freedom (SDOF) oscillator with mass m, damping d, and stiffness k. One way to extract power from a three-phase machine is to connect it to a servo drive, which interfaces the machine with a DC power bus (also called a "DC link"). The particular three-phase drive used for this paper is an S16A8 analog servo drive from Advanced Motion Controls. One of the main advantages of using a drive of this nature is that it is capable of four quadrant regenerative operation. However, there are several drawbacks to using an off-the-shelf drive for structural vibration applications. First of which is the fact that the switching frequency of the MOSFETs have been to tuned 33kHz and there is no way to adjust this setting. This switching frequency is more than an order of magnitude higher than what is necessary to track the desired currents that the drive will impose on the motor. For energy harvesting applications, it has been shown[17] that there is an optimal switching frequency of power electronic drives at which harvested power is maximized. Another drawback is due to the way in which the supply power is converted into logic power. An

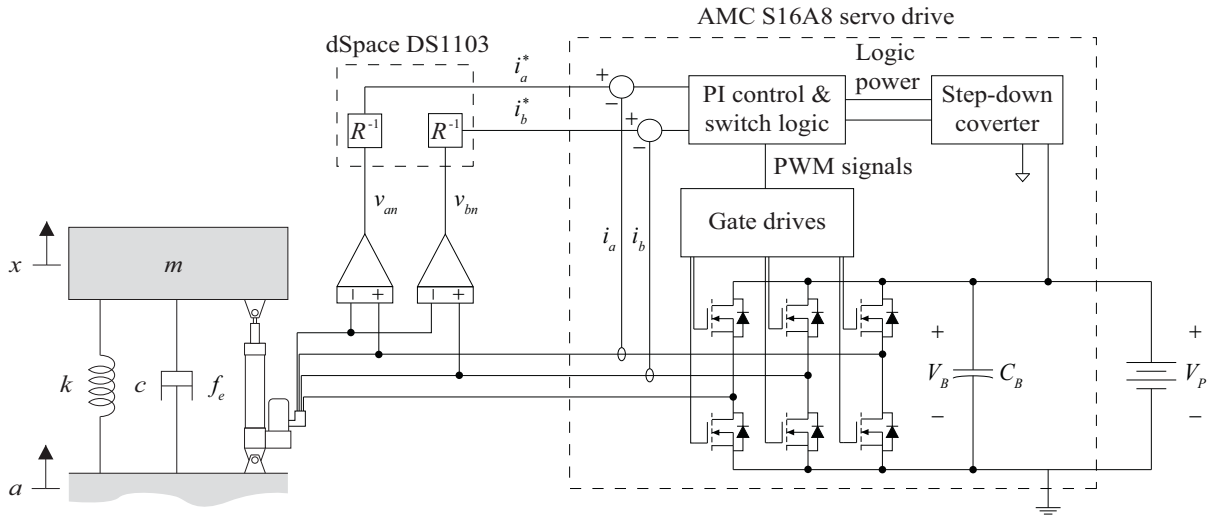

Figure 2. Diagram of an electromechanical transducer attached to a base-excited SDOF oscillator and interfaced with a three-phase analog servo drive.

analog step-down converter is used to reduce the supply voltage (which can range from 60-80V) to 12V to power various drive intelligence components. During this process a significant amount of power is being dissipated in the drive. Both of these drawbacks result in significant parasitic power losses, which can be reduced by using a drive that customized for the specific application.

3. DESIGN TRADEOFFS

The efficacy of the type of electromechanical transducer, as described here, will depend quite heavily on the combination of parameters for the screw conversion, motor, electronics, and the characteristics of the SDOF oscillator. It is important that all these components be taken into account in the design, especially because the combinations of parameters leading to the transducers effective use as a generator are very different from those that would be chosen to operate it as an actuator for position tracking, which is its conventional usage. In particular, there are several criteria which should be met for the device to operate as intended.

- Damping capability: The quantity

$$c_e^{short} = \frac{9K_e^2}{4Rl^2} \tag{6}$$

is approximately equal to the effective linear viscous damping contributed by the machine, when its terminals are shorted (i.e., when $v_{an} = v_{bn} = v_{cn} = 0$). When multiplied by the square of the linear velocity, this gives the maximum rate at which mechanical power can be extracted by the device (at a given v), before the internal dissipation in the motor exceeds power extraction. It is therefore the quantity most closely connected with the efficiency with which a combination of screw conversion (i.e., l) and machine (i.e., K_e and R) can manage a given amount of mechanical power. A good indicator of whether the hardware is properly sized for the application is therefore a measure of the fraction of critical damping imposed on the SDOF oscillator with this maximum viscosity imposed; i.e.,

$$\zeta_{max} = \frac{c_e^{short}}{2\sqrt{km}} \, . \tag{7}$$

For effective energy harvesting, the effective linear viscous damping imposed by the device should be considerably below c_e^{short}. Therefore, the fraction of critical damping desired for the SDOF oscillator should be considerably below ζ_{max}. As such, we define the first performance index for the device as

$$I_c = \zeta_{max} \tag{8}$$

with high values being more favorable. If the transducer is being used in structural control applications, ζ_{max} should be made as high as possible to give the device a wide range of variable damping.

- Force capability: The maximum force rating for the entire device will be approximately

$$f^{rat} = \min\{f^{rat}_{screw}, \tfrac{1}{l}T^{rat}_e\} \tag{9}$$

where f^{rat}_{screw} is the rated axial load of the screw and T^{rat}_e is the rated torque of the machine. Technically, if the device is being backdriven, the effective force rating can be amplified by a factor of $1/\eta$. This force should be sizable enough to have significant influence over the dynamics of the oscillator. So, for example, if the SDOF oscillator is excited by a base excitation near resonance with acceleration amplitude A_0, then a helpful index for the suitability of the device is the fraction

$$I_f = \frac{f^{rat}}{mA_0} \, . \tag{10}$$

Clearly, a higher value of I_f affords more control capability over the mass.

- Velocity amplification: Consider the case in which the servo drive in Fig. 2 is replaced by a full bridge diode rectifier. The diodes have a conduction voltage v_d, which must be overcome by the back-EMFs, before power can be transferred from the machine to the DC bus. This voltage threshold is almost unavoidable in power-electronics (unless the diodes are replaced with mechanical relays), and will persist even if more sophisticated electronics are used to control power extraction. As such, for the typical velocities to be experienced by the transducer, the voltages need to exceed this threshold by a comfortable margin. To evaluate this, we need to specify a design velocity, $\dot{x}_0$, for the transducer. Then, we define the index

$$I_v = \frac{3K_e\dot{x}_0}{2v_d l} \, . \tag{11}$$

This fraction is equal to 1 if the back-EMFs are just large enough to result in continuous conduction through the diode rectifier for their entire oscillatory cycle. Clearly, a suitable device should have $I_v \gg 1$.

- Inertia suppression: The last criterion has to do with the fact that there is a finite rotary inertia J in the system, and if the lead l is too small, this inertia will be reflected into the linear dynamics as an equivalent mass J/l^2, sizable enough so as to hamper the transducers dynamics. Indeed, this effect can often be the limiting factor in the choice of lead l. Thus, the index

$$I_m = \frac{ml^2}{J} \tag{12}$$

is critical to the suitability of the transducer, and design parameters should be chosen such that $I_m \gg 1$.

For example, the transducer in Fig. 1(a) has relevant properties as listed in Table 1. Note that the design values are also given, for a 400kg mass with a 2s natural period, driven by a 0.5g acceleration, with a design displacement of 5cm. For these values, the four indices discussed above are $\{I_c, I_f, I_v, I_m\} = \{33.9, 0.548, 53.4, 17.3\}$.

Parameter	Value	Parameter	Value
K_e	0.77N-m/A	c_e^{short}	85130N-s/m
R	2.41Ω	f^{rat}	1076N
L	8.93×10^{-3}H	m	400kg
l	2.55×10^{-3}m/rad	k	3948N/m
f^{rat}_{screw}	7.2kN	$\dot{x}_0$	0.165m/s
T^{rat}_e	2.74N-m	A_0	4.91m/s^2
v_d	1.4V	ω_0	0.5 Hz
J	1.5×10^{-4}N-m-s^2		
B	1.2×10^{-4}N-m-s		

Table 1. Example design parameters for the EC3 ballscrew and AKM42E motor from Danaher Motion.

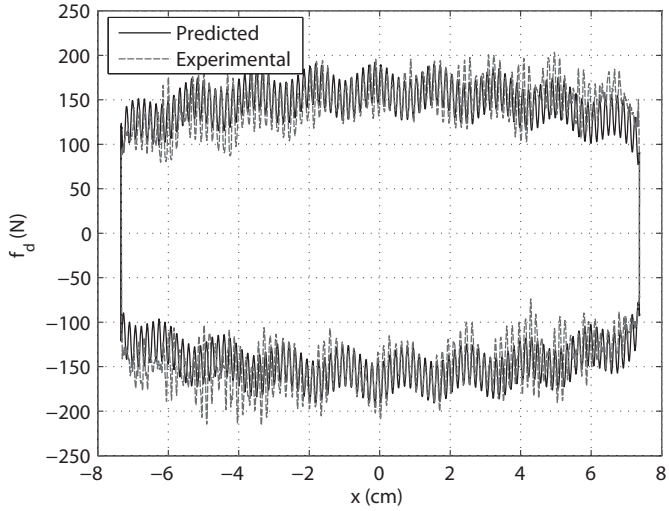

Figure 3. Experimentally measured friction force and an approximate model.

4. EXPERIMENTAL CHARACTERIZATION

To illustrate the characteristics of the electromechanical transducer described above, experiments were conducted in which the transducer displacement was controlled via a hydraulic actuator, and various response quantities were measured. The first test conducted was to characterize the friction force f_d. As mentioned previously, this force is the sliding friction force of the ballscrew. In most applications of precision ballscrews (which are for the purpose of positioning) this force is compensated for, via feedback, and oftentimes its characteristics are not extensively tested by manufacturers. To identify a model for f_d, the device position was made to oscillate sinusoidally at 0.1Hz, and at an amplitude of 7.5cm. The terminals of the motor were left open. The resulting opposing shaft force was measured using a load cell, and the components of the force due to the rotary inertia and damping (which had previously been identified) were subtracted away. The resultant force, f_d, is shown in Fig. 3.

An approximate analytical fit was made to the experimental data, with the functional form

$$f_d(t) = p_1 \left(1 + p_3 \sin\left(\lambda_1 x(t) + p_4\right) + p_5 \sin\left(\lambda_2 x(t) + p_6\right)\right) \operatorname{sgn}\left(\dot{x}(t)\right) + p_2 \dot{x}(t) \tag{13}$$

where λ_1 is $1/l$, and $\lambda_2 = 2\pi/r$ where $r = 0.17$cm is the diameter of the ball bearings. Note that this model also allows for additional viscous damping in the device. Empirical values for the constants are shown in Table 2, and result in reasonable agreement with the data. However, comparison of this fitted function with the experimental data illustrates that not all effects are accounted for. In particular, the device appears to have more Coulomb friction when it is fully retracted, compared to when it is fully extended.

Next, the forcing capability of the transducer was tested, for the case in which servo drive is used to dissipate energy like a simple resistor. These tests were conducted at 0.1Hz with an amplitude of 7.5cm and the results are presented in Fig. 4. Resistance values of 20Ω, 10Ω, 5Ω, 3Ω, 2Ω, and 1Ω in addition to the open circuit case were

Parameter	Value
p_1	98.9N
p_2	655N-s/m
p_3	0.0981
p_4	2.04
p_5	0.231
p_6	0.345

Table 2. Empirical parameters for f_d in equation (13).

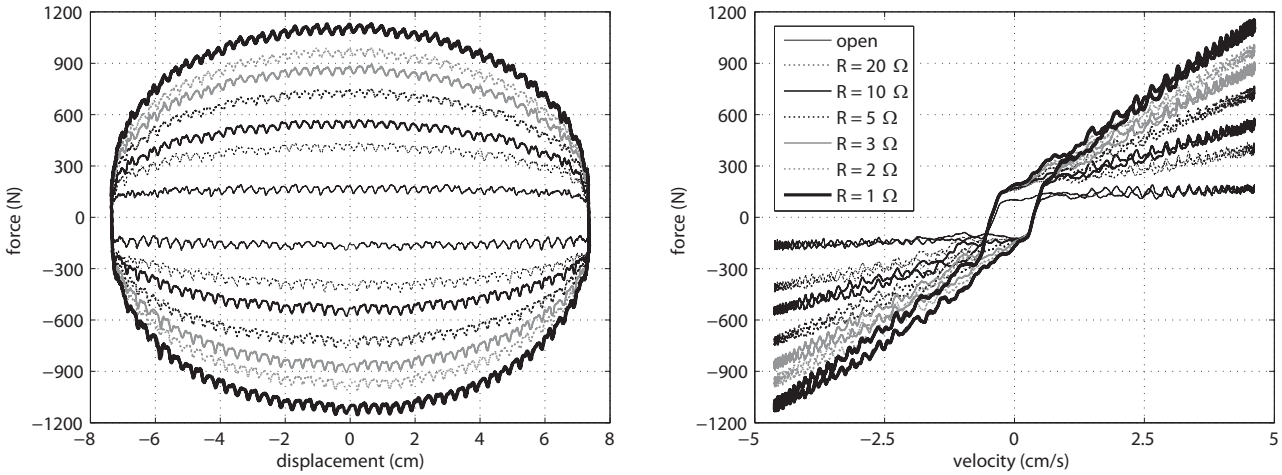

(a) Force vs. Displacement (b) Force vs. Velocity

Figure 4. Experimentally measured transducer force for various load resistances simulated by the servo drive.

chosen to illustrate the full force range of the device at this velocity. During the 1Ω test, the measured force is close to exceeding the maximum force rating f^{rat} for the device. It should be noted that all the hysteresis plots in Fig. 4(a) appear to exhibit predominately viscous damping behavior, with a Coulomb friction force threshold. We see that the nonlinear friction effects are present during each test. Resistance control could be used to compensate for the oscillations in the hysteresis plots, due to spatially-dependent Coulomb friction. However, this issue is beyond the scope of this paper, which is limited to a basic characterization and demonstration of the device.

Finally, a third test was conducted to illustrate rise time associated with the device reaching its rated force limit. A triangle wave with constant velocity, and with an amplitude of 5.25cm at 0.25Hz was used to demonstrate this concept. The plots presented in Fig. 5 show the results of this test. At the beginning of the test, the servo drive is used to simulate the device in open circuit mode. During the mid-way point of one of the oscillations, the servo drive is "switched on" and used to simulate a resistance value that results in the force reaching its rated value (in this case a 2Ω resistor was simulated). Fig. 5(b) shows a close-up view of measured force during this test. We note that the drive is "switched on" at 5.220s and it reaches its rated force at 5.226s, which is a

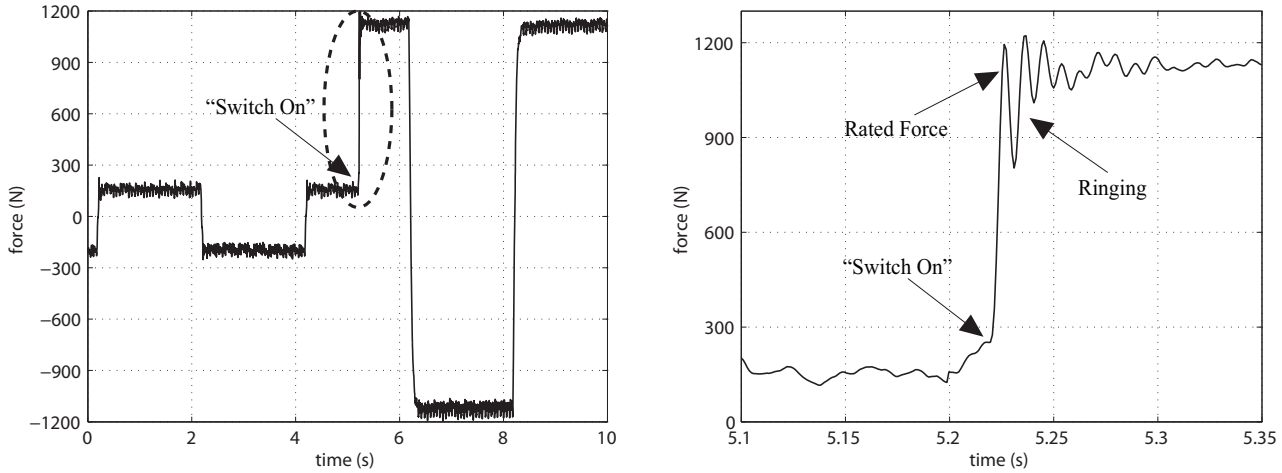

(a) Force vs. Time (b) Close-up view

Figure 5. Experimental force response for the transducer illustrating the rise time of the servo drive simulating a 2Ω resistive load.

rise time of approximately 6ms. This rise time is comparable to a magnetorheological (MR) damper of similar size and force rating.[18] However, it is clear that there is overshoot and ringing associated with using the servo drive this way. The oscillations occurring before the force measurement settles out is a result of the dynamic interaction between servo drive and the finite coil inductance of the motor. Because internal current tracking of the servo drive is accomplished by proportional control, a step in the current command causes a ringing effect in the force measurement for a brief period of time until the coils become fully magnetized. It would be possible to design a compensator using feedback to reduce these oscillations, but this is also beyond the scope of this paper.

5. IMPEDANCE MATCHING OF A TMD

We now present an example in which the electromechanical transducer and servo drive are attached to a TMD within a much larger structure. One of the simplest ways to optimize power from such an application is by resistive impedance matching. We assume that the TMD is excited at its base by a sinusoidal acceleration with amplitude A_0 and frequency w_0. First, we develop an analytical expression for the average power generated and use this expression to determine the optimal load resistance that should be imposed by the servo drive to maximize power. Next we compare the analytical model to our experimental system. The electromechanical transducer is back driven by a hydraulic actuator, which simulates the dynamics of TMD using real-time hybrid-testing (RTHT). RTHT is accomplished in dSpace by feeding back force measurements from the electromechanical transducer in real-time to a simulated disturbance and structure model. The force measurement and simulated disturbance force are summed together and used to excite the simulated structure. The output of the simulated structure is a displacement command signal, which is tracked by the digital controller that is used to operate the hydraulic actuator. Our experimental RTHT design follows the procedure in the study by Darby et al.[19]

The dynamics of the TMD coupled to the electromechanical transducer can be described by the following second order differential equation

$$\tilde{m}\ddot{x}(t) + \tilde{c}\dot{x}(t) + kx(t) + F_c \mathrm{sgn}\left(\dot{x}(t)\right) = mA_0 \sin(\omega_0 t) \tag{14}$$

where F_c is the amplitude of the Coulomb friction of the device (and is equal to p_1 in Table 2) and where

$$\tilde{m} = m + \frac{J}{l^2} \tag{15}$$

$$\tilde{c} = c + \frac{B}{l^2} + c_e \, . \tag{16}$$

We note that the viscous damping in the system, c, is equal to the identified parameter p_2 in Table 2. In addition, we note that the oscillatory components of the Coulomb friction derived in equation (13) are neglected in this analysis as they will have a negligible effect on the optimal resistance. Because the servo drive is being used to simulate a resistive load across the terminals of the transducer, we can express the electromechanical force as an additional viscous damping term in $\tilde{c}$. The effective electromechanical viscous damping from the transducer is

$$c_e = \frac{9K_e^2}{4l^2(R + R_L)} \tag{17}$$

where R_L is the load resistance simulated by the servo drive across the terminals of the three phases of the motor. Next, we derive an expression for the equivalent viscous damping from the Coulomb friction. This can be accomplished through an energy balance approach where we set the amount of energy dissipated during one oscillation from the Coulomb friction equal to the amount of energy dissipated by an equivalent viscous damper. This quantity can be expressed as

$$c_{eq} = \frac{4F_c}{\pi \dot{X}} \tag{18}$$

where $\dot{X}$ is the velocity amplitude.

The next step is derive an expression for the velocity amplitude of the system in (14) through harmonic balance. This expression can be written as

$$\dot{X} = \frac{mA_0\omega_0}{\sqrt{(-\tilde{m}\omega_0^2 + k)^2 + (\tilde{c} + c_{eq})^2\omega_0^2}} \, . \tag{19}$$

Since c_{eq} depends on $\dot{X}$, the expression in (19) is quadratic in $\dot{X}$. Substituting the expression for c_{eq} in (18) into (19) and solving for $\dot{X}$ results in

$$\dot{X} = \frac{-4\tilde{c}F_c\omega_0^2 + \sqrt{\omega_0^2\left(-16F_c^2\left(-\tilde{m}\omega_0^2+k\right)^2 + A_0^2m^2\pi^2\left(\tilde{c}^2\omega_0^2 + \left(-\tilde{m}\omega_0^2+k\right)^2\right)\right)}}{\pi\left(\tilde{c}^2\omega_0^2 + \left(-\tilde{m}\omega_0^2+k\right)^2\right)} \tag{20}$$

where we have thrown out the negative root. We can now express the average total power generated during one oscillation as a function of the back-emf of the motor; i.e.,

$$\bar{P}_{total} = \frac{\omega_0}{2\pi}\int_0^{\frac{2\pi}{\omega_0}} \frac{e_q^2}{R+R_L}\, dt \tag{21}$$

where $e_q = \frac{3K_e}{2l}\dot{x}(t)$ is the quadrature back-emf of the motor. Therefore, solving for $\bar{P}_{total}$ results in

$$\bar{P}_{total} = \frac{9\pi K_e^2\dot{X}^2}{8l^2(R+R_L)}\,. \tag{22}$$

Finally, we have that the average power generated across the load resistance R_L is

$$\bar{P}_{load} = \bar{P}_{total}\frac{R_L}{R+R_L} = \frac{9\pi K_e^2\dot{X}^2R_L}{8l^2(R+R_L)^2}\,. \tag{23}$$

It is possible to determine an analytical expression for the optimal resistive load by taking the partial derivative of $\bar{P}_{load}$ with respect to R_L, setting this quantity equal to zero, and solving for R_L. However, this analysis becomes extremely tedious due to the fact that the expression for average power in equation (23) is a fifth order polynomial in R_L.

The analytical expression for the average power generated across R_L is compared to the RTHT results in Fig. 6. It should be noted that the acceleration amplitude A_0 was limited to be 1m/s^2 so that the response of the TMD would be well within the displacement and velocity limits of the hydraulic actuator at 0.5Hz. We can see from this plot that we have excellent agreement between the predicted and experimental average power values over the range of load resistances. The optimal load resistance, as predicted by the analytical average power curve in Fig. 6, is 306.3Ω while the experimental results show that the maximum average power occurs at the 300Ω test.

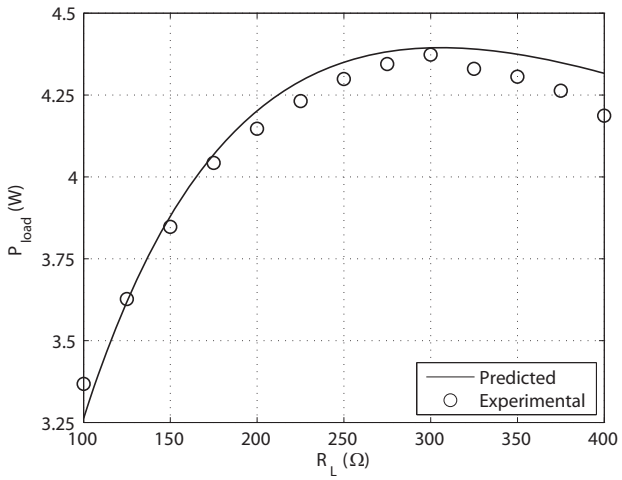

Figure 6. Comparison of predicted and experimental results of the average power over a range of resistive load values.

6. CONCLUSIONS

One of the three goals of this paper was to illustrate some of the design tradeoffs one faces, in the design of electromechanical transducers for use in structural control and large-scale energy harvesting applications. These design tradeoffs can be distilled down to a few criteria that should be used to balance various parameters of the machine, electronics, screw conversion, and structure, against each other. These criteria (or slight variations of them) hold with some generality, for applications of this technology in which the oscillation of the device is concentrated near a single frequency. The second goal of the paper was to illustrate experimental data on the validation of the use of such electromechanical transducers in the manner discussed here. Toward this end, we have illustrated that interfacing the transducer with a four quadrant servo drive results in a wide range of control by having the drive dissipate power like a simple resistive load. We have also demonstrated the extremely fast rise time that the device exhibits and that this rise time is comparable to a similar size magnetorheological damper. Finally, the third goal of this study was to derive analytical expression for the average power generated and use this expression to determine the optimal resistive load for the case where the transducer is interfaced with a TMD. Both the analytical model and the experimental system show similar results for the average power generated over the range of resistive loads. Additionally, the model is able to accurately predict the load resistance that maximizes power in the experimental system.

ACKNOWLEDGMENTS

Work by the first two authors was supported by NSF award CMMI-0747563. The views expressed in this article are those of the authors, and do not necessarily reflect those of the National Science Foundation.

REFERENCES

[1] Scruggs, J. T. and Iwan, W. D., "Control of a civil structure using an electric machine with semiactive capability," *Journal of Structural Engineering* **129**, 951–959 (2003).

[2] Scruggs, J. T. and Iwan, W. D., "Structural control with regenerative force actuation networks," *Journal of Structural Control and Health Monitoring* **12**, 25–45 (2004).

[3] Palomera-Arias, R., Connor, J. J., and Oschendorf, J. A., "Feasibility study of passive electromagnetic damping systems," *Journal of Structural Engineering* **134**, 164–170 (2008).

[4] Zuo, L., Scully, B., Shestani, J., and Zhou, Y., "Design and characterization of an electromagnetic energy harvester for vehicle suspensions," *Smart Materials & Structures* **19**, 045003 (2010).

[5] Nagode, C., Ahmadian, M., and Taheri, S., "Feasibility study of passive electromagnetic damping systems," in [*SPIE International Symposium on Smart Materials and Structures/NDE*], San Diego, CA (March 7-11 2010).

[6] Glynne-Jones, P., Tudor, M. J., Beeby, S. P., and White, N. M., "An electromagnetic, vibration-powered generator for intelligent sensor systems," *Sensors and Actuators A* **110**, 344–349 (2004).

[7] Roundy, S., Wright, P. K., and Rabaey, J., "A study of low level vibrations as a power source for wireless sensor nodes," *Journal of Computer Communications* **26**, 1131–1144 (2002).

[8] Ward, J. K. and Behrens, S., "Adaptive learning algorithms for vibration energy harvesting," *Smart Materials & Structures* **17**(3), 035025 (2008).

[9] Choi, Y. T. and Wereley, N. M., "Self-powered magnetorheological dampers," *Journal of Vibration and Acoustics* **131**, 044501 (2009).

[10] Anton, S. R. and Sodano, H. A., "A review of power harvesting using piezoelectric materials (2003-2006)," *Smart Materials and Structures* **16**, R1–R21 (2007).

[11] Priya, S. and Inman, D. J., eds., [*Energy Harvesting Technologies*] (2009).

[12] Mitcheson, P. D., Miao, P., Stark, B. H., Yeatman, E. M., Holmes, A. S., and Green, T. C., "Mems electrostatic micro-power generator for low frequency operation," *Sensors Actuators* **A115**, 523–529 (2004).

[13] Amirtharajah, R. and Chandrakasan, A. P., "Self-powered signal processing using vibration-based power generation," *IEEE Journal of Solid-State Circuits* **33**, 687–695 (1998).

[14] Scruggs, J. T., Cassidy, I. L., and Behrens, S., "Design and experimental characterization of a three-phase, 1kn regenerative actuator," in [*5th World Conference on Structural Control & Monitoring*], Tokyo, Japan (July 12-14 2010).

[15] Lefeuvre, E., Audigier, D., Richard, C., and Guyomar, D., "Buck-boost converter for sensorless power optimization of piezoelectric energy harvester," *IEEE Transactions on Power Electronics* **22**, 2018–2025 (2007).

[16] Kong, N., Ha, D. S., Erturk, A., and Inman, D. J., "Resistive impedance matching circuit for piezoelectric energy harvesting," *Journal of Intelligent Material Systems and Structures* **21**, 1293–1302 (2010).

[17] Ottman, G. K., Hofmann, H. F., and Lesieutre, G. A., "Optimized piezoelectric energy harvesting circuit using step-down converter in discontinuous conduction mode," *IEEE Transactions On Power Electronics* **18**, 696–703 (2003).

[18] Dyke, S. J., Spencer, B. F., Sain, M. K., and Carlson, J. D., "Modeling and control of magnetorheological dampers for seismic response reduction," *Smart Materials & Structures* **5**, 565–575 (1996).

[19] Darby, A. P., Blakeborough, A., and Williams, S., "Real-time substructure tests using hydraulic actuator," *Journal of Engineering Mechanics* **125**, 1133–1139 (1999).